Simple Model for Semipermeable Membrane: Donnan Equilibrium

Felipe Jiménez-Ángeles and Marcelo Lozada-Cassou*

Programa de Ingeniería Molecular, Instituto Mexicano del Petróleo, Lázaro Cárdenas 152, 07730 México, D. F., México, Departamento de Física, Universidad Autónoma Metropoloitana-Iztapalapa, Apartado Postal 55-334, 09340 D.F. México

Received: June 26, 2003; In Final Form: November 12, 2003

We study a model for macroions in an electrolyte solution, confined by a semipermeable membrane. The membrane finite thickness is considered, and both membrane surfaces are uniformly charged. The model explicitly includes electrostatic and size particles correlations. Our study is focused on the adsorption of macroions on the membrane surface and on the osmotic pressure. The theoretical prediction for the osmotic pressure shows a good agreement with experimental results.

1. Introduction

The physics of two ionic solutions separated by a semipermeable membrane is of wide interest in cell biology and colloids science.[1,2,3] A thermodynamical study of this problem was first carried out by Donnan,[4,5] considering the two fluids phases (here referred as α and β) in the following way: (i) the α phase contains two (small) ionic species and (ii) the β phase contains the same ionic species as the α phase plus one macroion species. The two fluid phases are separated by a membrane which is permeable to the small ions and impermeable to macroions; therefore, they interchange small ions, whereas macroions are restricted to the β phase. The permeability condition is imposed by assuming (in both phases) a constant chemical potential of the permeating species. In this simple model, Donnan derived an expression for the osmotic pressure (in terms of the macroions charge and excluded volume, and the salt valence and concentration at both sides of the membrane) which well describes systems close to ideality. Historically, this problem has been known as Donnan equilibrium. More recently, some theories have been proposed to interpret osmotic pressure data.[6,7] These theories phenomenologically consider macroion−macroion and ion−macroion many-body interactions and provide a better fit for the osmotic pressure of macroions solutions than Donnan theory.

The surface of a biological membrane has a net charge when it is in aqueous solution;[1] thus, at a fluid−membrane interface, a broad variety of phenomena occur. It is known that ionic solutions in the neighborhood of a charged surface produce an exponentially decaying charge distribution, known as the electrical double layer. Low-concentrated solutions of monovalent ions are well described by the Gouy−Chapman theory (Poisson−Boltzmann equation).[8,9] However, multivalent ions display important deviations from this picture[10] and more powerful theories from modern statistical mechanics (such as molecular simulation,[11−13] density functionals,[14−16] and integral equations[17−21]) have been implemented for studying ions adsorption and interfacial phenomena. Macroions adsorption is a subject of current interest: In molecular engineering, the macroions adsorption mechanisms are important in self-assembling polyelectrolyte layers on a charged substrate[22] and novel colloids stabilization mechanisms.[23]

By means of integral equations, a previous study of Donnan equilibrium has been carried out by Zhou and Stell.[24,25] They used a method proposed by Henderson,[17] which can be described as follows: starting from a semipermeable spherical cavity,[26] the planar membrane is obtained taking the limit of infinite cavity radius. Within this model, they obtained the charge distribution and mean electrostatic potential. However, due to the approximations used, they end up just with the integral version of the linear Poisson−Boltzmann equation. A general shortcoming of the Poisson−Boltzmann equation is that ionic size effects (short range correlations) are completely neglected; as a consequence, the description of interfacial phenomena and computation of thermodynamical properties is limited and valid only for low values of charge and concentration.

From previous studies of two fluid phases separated by a *permeable* membrane, it is known that the adsorption phenomena are strongly influenced by the membrane thickness.[27−29] On the other hand, short-range correlations influence effective colloid−colloid interaction,[30−34] thermodynamical properties,[35] and adsorption phenomena[36,37] in colloidal dispersions. From these antecedents, it is seen that there are several relevant aspects not considered in previous studies of Donnan equilibrium which deserve a proper consideration. In this study, we consider explicitly the following effects: many-body (short and long range) correlations, the membrane thickness, and the surface charge densities on each of the membrane faces. We use *simple* model interactions, and our study is carried out by means of integral equations. The theory gives the particles distribution in the neighborhood of the membrane, from which the osmotic pressure is calculated. There are two points that we will address in this study: the adsorption of macroions at the membrane surface and the computation of the osmotic pressure for macroions solutions. Concerning the adsorption phenomena, we observe a broad variety of phenomena: charge reversal, charge inversion, and macroions adsorption on a like-charged surface due to the fluid−fluid correlation. The computed osmotic pressure is compared with experimental results for a protein solution, obtaining a good agreement over a wide interval of concentrations.

The paper is organized as follows. In section 2, we describe the integral equations method and the membrane and fluid

* To whom correspondence should be addressed. E-mail: marcelo@imp.mx

10.1021/jp035829p CCC: $27.50
Published on Web 01/13/2004

models. In the same section, we derive the *hypernetted chain/mean spherical* (HNC/MS) integral equations for the semipermeable membrane and the equations to compute the osmotic pressure. In section 3, results are presented and discussed, and finally, in section 4, some conclusions are given.

2. Theory

2.1. Integral Equations for Inhomogeneous Fluids. The method that we use to derive integral equations for inhomogeneous fluids makes use of a simple fact: In a fluid, an external field can be considered as a particle in the fluid, i.e., as one more species infinitely dilute. This statement is valid in general; however, it is particularly useful in the statistical mechanics theory for inhomogeneous fluids[18,38] described below.

The multicomponent Ornstein−Zernike equation for a fluid made up of $n + 1$ species is

$$h_{ij}(\mathbf{r}_{21}) = c_{ij}(\mathbf{r}_{21}) + \sum_{m=1}^{n+1} \rho_m \int h_{im}(\mathbf{r}_{23}) c_{mj}(\mathbf{r}_{13})\, \mathrm{d}\upsilon_3 \qquad (1)$$

where ρ_m is the number density of species m, $h_{ij}(\mathbf{r}_{21}) \equiv g_{ij}(\mathbf{r}_{21}) - 1$ and $c_{ij}(\mathbf{r}_{21})$ are the total and direct correlation functions for two particles at $\mathbf{r}_2$ and $\mathbf{r}_1$ of species i and j, respectively; with $g_{ij}(\mathbf{r}_{21})$ the pair distribution and $\mathbf{r}_{21} = \mathbf{r}_2 - \mathbf{r}_1$. Among the most known closures between $h_{ij}(\mathbf{r}_{21})$ and $c_{ij}(\mathbf{r}_{21})$ used to solve eq 1, we have[39]

$$c_{ij}(\mathbf{r}_{21}) = -\beta u_{ij}(\mathbf{r}_{21}) + h_{ij}(\mathrm{r}_{21}) - \ln g_{ij}(\mathbf{r}_{21}) \qquad (2)$$

$$c_{ij}(\mathbf{r}_{21}) = -\beta u_{ij}(\mathbf{r}_{21}) \text{ for } r_{21} \equiv |\mathbf{r}_{21}| \geq a_{ij} \qquad (3)$$

Equations 2 and 3 are known as the hypernetted chain (HNC) and the mean spherical (MS) approximations, respectively; $u_{ij}(\mathbf{r}_{21})$ is the direct interaction potential between two particles of species i and j, a_{ij} is their closest approach distance, and $\beta \equiv 1/k_B T$. Some more possibilities to solve eq 1 are originated by considering a closure for $c_{ij}(\mathbf{r}_{21})$ in the first term of eq 1 and a different one for $c_{mj}(\mathbf{r}_{13})$ in the second term of eq 1, giving rise to hybrid closures.

To derive integral equations for inhomogeneous fluids, we let an external field to be one of the fluid species, say the $(n + 1)$ species (denoted as the γ-species), which is required to be infinitely dilute, i.e., $\rho_\gamma \rightarrow 0$. Therefore, the total correlation function between a γ species particle and a j species particle is given by

$$h_{\gamma j}(\mathbf{r}_{21}) = c_{\gamma j}(\mathbf{r}_{21}) + \sum_{m=1}^{n} \rho_m \int h_{\gamma m}(\mathbf{r}_{23}) c_{mj}(\mathbf{r}_{13})\, \mathrm{d}\upsilon_3 \quad \text{with } j = 1, ..., n \qquad (4)$$

The total correlation functions for the remaining species satisfy a n-component Ornstein−Zernike equation as eq 1 (with no γ species) from which $c_{mj}(\mathbf{r}_{13})$ is obtained. In this scheme, the pair correlation functions, $g_{\gamma i}(\mathbf{r}_{21})$, is just the inhomogeneous one-particle distribution function, $g_i(\mathbf{r}_1)$, for particles of species j under the influence of an external field. Thus, $h_{\gamma j}(\mathbf{r}_{21})$ and $c_{\gamma j}(\mathbf{r}_{21})$ can be replaced with $h_j(\mathbf{r}_1) \equiv g_j(\mathbf{r}_1) - 1$ and $c_j(\mathbf{r}_1)$, respectively. Hence, the inhomogeneous local concentration for the j species is given by

$$\rho_j(\mathbf{r}_1) = \rho_j g_j(\mathbf{r}_1) \qquad (5)$$

By using the HNC closure (eq 2) for $c_{\gamma j}(\mathbf{r}_{21})$ in eq 4, we get

$$g_j(\mathbf{r}_1) = \exp\{-\beta u_j(\mathbf{r}_1) + \sum_{m=1}^{n} \rho_m \int h_m(\mathbf{r}_3) c_{mj}(\mathbf{r}_{13})\, \mathrm{d}\upsilon_3\} \qquad (6)$$

where the subindex γ has been omitted for consistency with eq 5. In our approach, $c_{mj}(\mathbf{r}_{13})$ in the integral of eq 6 is given by the direct correlation function for a n-component *homogeneous fluid*; that is, $c_{mj}(\mathbf{r}_{13})$ is obtained from eq 1 using one of the closures provided by eqs 2 and 3. For the present derivation, we will use $c_{mj}(\mathbf{r}_{13})$ obtained with the MS closure (eq 3). Therefore, eq 6 becomes the hypernetted chain/mean spherical (HNC/MS) integral equations for an inhomogeneous fluid. This equation has shown to be particularly successful in the case of inhomogeneous charged fluids when it is compared with molecular simulation data.[40,41,42,43]

2.2. Semipermeable Membrane and Fluid Models. The membrane is modeled as a planar hard wall of thickness d, and charge densities σ_1 and σ_2, on each surface, and separates two fluid phases, referred as α and β. In Figure 1, σ_1 and the α phase are at the left-hand side, whereas σ_2 and the β phase are at the right-hand side. The fluid phased are made up in the following way: (i) The α phase is a two component electrolyte, considering the components to be hard spheres of diameter a_i with a centered point charge $q_i = z_i e$ (with z_i and e being the ionic valence and the proton's charge, respectively) and $i = 1$ and 2 standing for the species number. The solvent is considered as a uniform medium of dielectric constant ϵ. (ii) The β phase is considered in the same way as the α phase (same solvent dielectric constant and containing the same ionic species) plus one more species (species 3) of diameter a_3 and charge q_3. For simplicity, we have considered that the membrane dielectric constant is equal to that of the solvent. In addition, it is considered that

$$a \equiv a_1 = a_2 \leq a_3 \qquad (7)$$

Hence, we refer to the third species as the macroion species. Two ions of species m and j with relative position r, interact via the following potential

$$u_{mj}(r) = \begin{cases} \infty & \text{for } r < a_{mj} \\ \dfrac{z_m z_j e^2}{\epsilon r} & \text{for } r \geq a_{mj} \end{cases} \qquad (8)$$

with $m, j = 1, ..., 3$ and $a_{mj} \equiv (a_m + a_j)/2$. Far away from the membrane, each phase is homogeneous and neutral, thus the bulk electroneutrality condition is

$$\sum_{i=1}^{2} z_i \rho_i^{\alpha} = \sum_{i=1}^{3} z_i \rho_i^{\beta} = 0 \qquad (9)$$

with ρ_i^{α} and ρ_i^{β} being the bulk concentrations of the i species in the α and β phases, respectively. The charge on the membrane is compensated by an induced charge in the fluid (per unit area), σ':[44,45]

$$\sigma' \equiv \sigma^{\alpha} + \sigma^{\beta} = -\sigma_T \qquad (10)$$

with $\sigma_T = \sigma_1 + \sigma_2$ and being σ^{α} and σ^{β} the induced of charge in the α phase and β phase, respectively, and are given by

$$\sigma^{\alpha} = \int_{-\infty}^{-d/2} \rho_{el}(x)\, \mathrm{d}x \qquad (11)$$

and

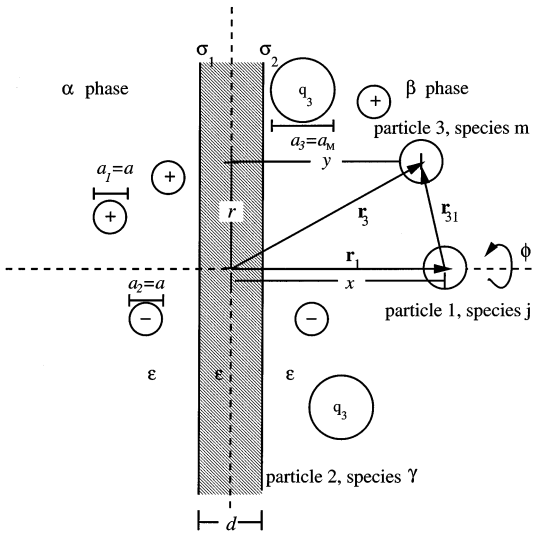

Figure 1. Schematic representation for a model macroions solution confined by a semipermeable membrane. For the integration of eq 17, it is considered the *axial* symmetry around the $\mathbf{r}_1$ vector where we fix a cylindrical coordinates system (ϕ, r, y).

$$\sigma^{\beta} = \int_{d/2}^{\infty} \rho_{el}(x)\, \mathrm{d}x \tag{12}$$

where

$$\rho_{el}(x) \equiv e\sum_{m=1}^{3} z_m \rho_m(x) \tag{13}$$

is the local charge density profile. It should be pointed out that, in general, $-\sigma^{\alpha} \neq \sigma_1$ and $-\sigma^{\beta} \neq \sigma_2$; that is, there is a violation of the local electroneutrality condition.[27,28,29,41,45] Because of the symmetry of the system, in eqs 11−13, the particles reduced concentration profile ($g_j(\mathbf{r}_1)$) depends only on the perpendicular position to the membrane, x, i.e., $g_j(\mathbf{r}_1) = g_j(x)$. Hence, the local concentration profile is $\rho_m(x) = \rho_m g_m(x)$.

According to the integral equations method outlined in section 2.1, the membrane is considered as the fluid species labeled as species γ (see Figure 1). The interaction potential between the membrane and a j-species particle depends only on the particle position, x, referred to a coordinates system with origin in the middle of the membrane and measured perpendicularly. Thus, we write $u_j(\mathbf{r}_1) = u_j(x)$, which is split as $u_j(x) = u_j^{\mathrm{el}}(x) + u_j^{*}(x)$, with $u_j^{\mathrm{el}}(x)$ being the direct electrostatic potential and $u_j^{*}(x)$ the hard-core interaction. The former can be found from Gauss' law, i.e.

$$-\beta u_j^{\mathrm{el}}(x) = \begin{cases} \dfrac{2\pi}{\epsilon} z_j e\beta\sigma_T (x - L) & \text{for } x \geq \dfrac{d}{2} \\ \dfrac{2\pi}{\epsilon} z_j e\beta[\sigma_T(-x - L) - (\sigma_1 - \sigma_2)d] & \text{for } x \leq \dfrac{-d}{2} \end{cases} \tag{14}$$

where L is the location of a reference point.

The hard-core interaction is given by

$$u_j^{*}(x) = \begin{cases} \infty & \text{for } |x| < \dfrac{d + a}{2} \\ 0 & \text{for } |x| \geq \dfrac{d + a}{2} \end{cases} \tag{15}$$

for $j = 1$ and 2. For the membrane impermeable species ($j = 3$)

$$u_3^{*}(x) = \begin{cases} \infty & \text{for } x < \dfrac{d + a_3}{2} \\ 0 & \text{for } x \geq \dfrac{d + a_3}{2} \end{cases} \tag{16}$$

This potential imposes $g_3(x) = 0$ for $x \leq (d + a_3/2)$.

In the integral of eq 6, we use the MS expression of $c_{mj}(r_{13})$ for a primitive model *bulk* electrolyte, i.e.

$$c_{mj}(r_{13}) = \begin{cases} -\beta u_{mj}^{\mathrm{el}}(r_{13}) = -\beta \dfrac{z_m z_j e^2}{\epsilon r} & \text{for } r_{13} \geq a_{mj} \\ c_{mj}^{\mathrm{sr}}(r_{13}) + c_{mj}^{\mathrm{hs}}(r_{13}) & \text{for } r_{13} < a_{mj} \end{cases} \tag{17}$$

where $r_{13} \equiv |\mathbf{r}_{13}|$ is the relative distance between two ions of species m and j. The particles short-range correlations are considered through the *bulk* direct correlation functions, $c_{mj}^{\mathrm{sr}}(r_{13})$ and $c_{mj}^{\mathrm{hs}}(r_{13})$. The explicit form of these functions is given in Appendix A. Because of the symmetry of the system, it is convenient to use cylindrical coordinates in the integral of eq 6, and we can analytically integrate in the ϕ and r variables (see Figure 1); that is, we consider a cylindrical coordinates system where $r_{13}^2 = x^2 + r^2 + y^2 - 2xy$ and $\mathrm{d}\upsilon_3 = \mathrm{d}\phi r\, \mathrm{d}r\, \mathrm{d}y$. After a lengthy algebra, from eq 6, we get[44,45]

$$\begin{aligned} g_j(x) = \exp\Bigg\{ & \frac{2\pi}{\epsilon} z_j e\beta(\sigma_1 + \sigma_2)|x| - 2\pi A_j(x) + \\ & 2\pi\sum_{m=1}^{2} \rho_m \int_{-\infty}^{-(d+a_m/2)} h_m(y) G_{mj}(x, y)\, \mathrm{d}y + \\ & 2\pi\sum_{m=1}^{3} \rho_m \int_{(d+a_m/2)}^{\infty} h_m(y) G_{mj}(x, y)\, \mathrm{d}y + \\ & 2\pi z_j \frac{e^2\beta}{\epsilon} \sum_{m=1}^{2} z_m \rho_m \int_{-\infty}^{-(d+a_m/2)} g_m(y)[y + |x - y|]\, \mathrm{d}y + \\ & 2\pi z_j \frac{e^2\beta}{\epsilon} \sum_{m=1}^{3} z_m \rho_m \int_{(d+a_m/2)}^{\infty} h_m(y)[y + |x - y|]\, \mathrm{d}y \Bigg\} \end{aligned} \tag{18}$$

The first and third integrals include $h_j(y) = g_j(y) - 1$ for particles in the α phase, whereas in the second and fourth integrals, $h_j(y)$ are for particles in the β phase. Notice the different summation limits due to the different phase composition. We have defined

$$G_{mj}(x, y) = L_{mj}(x, y) + K_{mj}(x, y) \tag{19}$$

$$L_{mj}(x, y) = \int_{|x-y|}^{\infty} c_{mj}^{\mathrm{sr}}(r_{13}) r_{13} dr_{13} = \frac{e^2\beta}{\epsilon} D_{mj}(x, y) \tag{20}$$

$$K_{mj}(x, y) = \int_{|x-y|}^{\infty} c_{mj}^{\mathrm{hs}}(r_{13})\, r_{13} dr_{13} \tag{21}$$

and

$$\begin{aligned} A_j(x) = & \rho_3 \int_{-\infty}^{(d+a_3/2)} G_{3j}(x, y)\, \mathrm{d}y + \\ & \sum_{m=1}^{2} \rho_j \int_{-(d+a_m/2)}^{(d+a_m/2)} G_{mj}(x, y)\, \mathrm{d}y + z_j z_3 \rho_3 \frac{\beta e^2}{\epsilon} \int_{(d+a/2)}^{(d+a_3/2)} [y + \\ & |x - y|]\, \mathrm{d}y + z_j e \frac{\beta d}{\epsilon} (\sigma_1 - \sigma_2)\Theta(x + d/2) \end{aligned} \tag{22}$$

with $\Theta(x)$ the step function, defined as

$$\Theta(x) = \begin{cases} 0 & \text{for } x < 0 \\ 1 & \text{for } x \geq 0 \end{cases} \tag{23}$$

The expressions for the kernels, $K_{mj}(r, y)$ and $D_{mj}(x, y)$, are given in Appendix A. Notice that in the integrals of eqs 18 and 22 the fluid in the α phase is correlated to that of the β phase, v. gr., in the integrals of eq 18, a particle at $x > (d+a_m/2)$, considers the direct and total correlation functions at both sides of the membrane.

From the solution of eq 18 one obtains the reduced concentration profile, $\rho_j(x) = \rho_j g_j(x)$. The *bulk* concentrations of species j, at the α and β phases (ρ_j^{α} and ρ_j^{β}), are given by

$$\rho_j^{\beta} = \lim_{x\to\infty} \rho_j g_j(x) \tag{24}$$

and

$$\rho_j^{\alpha} = \lim_{x\to-\infty} \rho_j g_j(x) \tag{25}$$

respectively. At the β phase, $g_j(x) \to 1$ as $x \to \infty$ then $\rho_j^{\beta} = \rho_j$. On the other hand, in the α phase (for $x < 0$), $\lim_{x\to-\infty} g_j(x) \neq 1$. It must be pointed out that the electrolyte bulk concentrations at the α phase (ρ_j^{α}, for $j = 1$ and 2) are *a result from our theory*, and we have numerically demonstrated that they satisfy the bulk electroneutrality condition, eq 9.

2.3. Computation of the Osmotic Pressure: Contact Theorem. Let us consider a slice of fluid of width dx, area of its faces, A, parallel to the membrane and located at x. From a straightforward force balance, the force on the slice in the x direction, dF_x, is given by[45,46]

$$\mathrm{d}F_x(x) = E_x(x)\,\mathrm{d}Q + A\,\mathrm{d}p(x) \tag{26}$$

being $E_x(x)$ the electric field in the x direction at x, dQ the total charge in the fluid slice, and d$p(x)$ the pressure difference at the two faces. The fluid−membrane short-range interaction terms are not included in eq 26. In our model, such terms are of *hard-core* nature and will be considered as boundary conditions when eq 26 is integrated. However, if short-range interactions are of different nature, additional terms should appear in eq 26.

Taking into account that

$$E_x(x) = -\frac{\partial\psi(x)}{\partial x} \tag{27}$$

and using Poisson's equation

$$\frac{\partial^2\psi(x)}{\partial x^2} = -\frac{4\pi}{\epsilon}\rho_{el}(x) \tag{28}$$

we write

$$\mathrm{d}Q = A\rho_{el}(x)\,\mathrm{d}x = -\frac{A\epsilon}{4\pi}\left(\frac{\partial^2\psi(x)}{\partial x^2}\right)\mathrm{d}x \tag{29}$$

Thus, we rewrite eq 26 as

$$\mathrm{d}F_x(x) = \frac{A\epsilon}{4\pi}\left(\frac{\partial\psi(x)}{\partial x}\right)\left(\frac{\partial^2\psi(x)}{\partial x^2}\right)\mathrm{d}x + A\,\mathrm{d}p(x) \tag{30}$$

or equivalently

$$\mathrm{d}F_x(x) = \frac{A\epsilon}{8\pi}\frac{\partial}{\partial x}\left(\frac{\partial\psi(x)}{\partial x}\right)^2\mathrm{d}x + A\,\mathrm{d}p(x) \tag{31}$$

Considering that in equilibrium $\mathrm{d}F_x(x) = 0$ and integrating eq 31 in the interval $[d/2,\infty)$ with the boundary condition

$$\lim_{x\to\infty}\frac{\partial\psi(x)}{\partial x} = 0 \tag{32}$$

we obtain

$$\frac{\epsilon}{8\pi}\left(\frac{\partial\psi(x)}{\partial x}\right)_{x=x_0}^{2} + (p_0^{\beta} - \Pi^{\beta}) = 0 \tag{33}$$

where $\Pi^{\beta} \equiv \lim_{x\to\infty} p(x)$ is the bulk fluid pressure and the expression for the pressure on the membrane right surface, $p_0^{\beta} \equiv p(0)$, is given by

$$p_0^{\beta} = k_B T \rho_T^{\beta}(0) = k_B T \sum_{i=1}^{3} \rho_i g_i\left(\frac{d + a_i}{2}\right) \tag{34}$$

where $\rho_T^{\beta}(0) = \sum_{i=1}^{3} \rho_i(d + a_i/2)$. Equation 34 is an *exact* relationship which can be obtained by considering the force on the fluid (at the contact plane) exerted by the *hard* wall.[47] From basic electrostatics, we have

$$\frac{\epsilon}{4\pi}\left(\frac{\partial\psi(x)}{\partial x}\right)_{x=d/2} = \int_{d/2}^{\infty} \rho_{el}(x)\,\mathrm{d}x \tag{35}$$

Thus, using eqs 33−35, we can write

$$\Pi^{\beta} = \frac{2\pi}{\epsilon}\left[\int_{d/2}^{\infty}\rho_{el}(x)\,\mathrm{d}x\right]^2 + k_B T\sum_{i=1}^{3}\rho_i g_i\left(\frac{d + a_i}{2}\right)$$
$$= \frac{2\pi}{\epsilon}(\sigma^{\beta})^2 + p_0^{\beta} \tag{36}$$

where the first term can be identified as the Maxwell stress tensor and we have used the definitions given in eqs 11 and 12. A similar expression is obtained for the bulk pressure in the α phase

$$\Pi^{\alpha} = \frac{2\pi}{\epsilon}\left[\int_{-\infty}^{-d/2}\rho_{el}(x)\,\mathrm{d}x\right]^2 + k_B T\sum_{i=1}^{2}\rho_i g_i\left(-\frac{d + a_i}{2}\right)$$
$$= \frac{2\pi}{\epsilon}(\sigma^{\alpha})^2 + p_0{}^{\alpha} \tag{37}$$

The osmotic pressure, Π, is defined as

$$\Pi = \Pi^{\beta} - \Pi^{\alpha} \tag{38}$$

From eqs 36 and 37, eq (38) becomes

$$\Pi = \frac{2\pi}{\epsilon}\{[\sigma^{\beta}]^2 - [\sigma^{\alpha}]^2\} + k_B T\sum_{i=1}^{3}\rho_i g_i\left(\frac{d + a_i}{2}\right) - k_B T\sum_{i=1}^{2}\rho_i g_i\left(-\frac{d + a_i}{2}\right) \tag{39}$$

Because of the fluid−fluid correlation across a thin membrane, the induced charge densities (σ^{α} and σ^{β}) and $g_i(\pm(d + a_i/2))$ in general depend on the fluid conditions (ρ_i, z_i, a_i, with $i = 1$, ..., 3) and on the membrane parameters (σ_1, σ_2, and d).[27,28,29] The computed value of Π (using σ^{α}, σ^{β}, and $g_i(\pm(d + a_i/2))$ from

HNC/MS), however, does *not* depend on the membrane parameters. We have numerically corroborated this fact by computing Π for several values of σ_1, σ_2, and d. This is physically appealing since the pressure can only depend on the bulk fluid conditions at both sides of the membrane. However, we had to do very precise calculations of $g_i(x)$, particularly in the neighborhood of $x = \pm (d + a_i/2)$, to prove the above statement.

Equation 39 is an *exact* theorem to compute the osmotic pressure, Π, in terms of microscopic quantities. A similar expression for the osmotic pressure was derived by Zhou and Stell.[25] However, the differences between the current derivation and that of those authors are due to the ion−membrane short-range interactions (not considered by them). If we use, in the Zhou and Stell theory, the hard wall interaction between the permeable ions and the membrane (provided by eq 15), we recover eq 39.

3. Results and Discussion

Several physical effects determine particles adsorption on the charged membrane. One of the most relevant is the membrane-particle direct interaction energy, which, at the surface, is given by

$$U_i = q_i u_i\left(\frac{a_i}{2}\right) = \frac{2\pi q_i \sigma}{\epsilon}\left(L - \frac{a_i}{2}\right) \tag{40}$$

with L being the location of a reference point. The more negative the value of U_i, the more energetically favorable is the particles adsorption. Many body correlations also play an important role in the adsorption phenomena and are responsible for the surface−particle forces of nonelectrostatic origin. Although it is not possible to sharply distinguish the origin of correlations, we assume that the particles volume fraction

$$\eta_T \equiv \frac{\pi}{6}\sum_i \rho_i a_i^3 \tag{41}$$

quantifies the contribution of short-range correlations. To quantify the effect of the Coulombic interaction (long-range correlations), we define the parameter

$$\xi_{ij} = \beta q_i q_j / \epsilon a_{ij} \tag{42}$$

In the discussion, the effects produced by varying the fluid parameters (a_i, z_i, and ρ_i, with $i = 1, ..., 3$) will be associated with the increment (or decrement) of the contributions arising from short and long-range correlations (η_T and ξ_{ij}).

For our discussion, it is useful to remark the following concepts: When the amount of adsorbed charge exceeds what is required to cancel the surface charge, a surface *charge reversal* (CR) is said to occur. As a consequence, at a certain distance from the surface, the electric field is inverted. Hence, next to the CR layer, a second layer of ions (with same charge sign as that of the surface) is formed, producing a *charge inversion* (CI) of the electrical double layer.[48,49] Such a denomination (charge inversion) is originated from the fact that ions invert their role in the diffuse layer. In the past, we have shown that charge reversal and charge inversion are many body effects and are induced by a compromise between short-range correlations (η_T) and electrostatic long-range correlations (ξ_{ij}).[37,50]

The HNC/MS equations for a semipermeable membrane, eq 18, are numerically solved using a finite element technique.[51,52] From the solution of HNC/MS equations, the reduced concentration profiles (RCPs), $g_j(x)$, are obtained. In the discussion, we adopted the following notation: $z_1 = z_+$, $z_2 = z_-$, and $z_3 = z_M$ for the number valence of cations, anions and macroions, respectively; idem for ρ_i and a_i. In all our calculations, we have used fixed values of $T = 298$ K, $\epsilon = 78.5$, and $a = 4.25$ Å. The effects of salt valence, macroions size, and membrane surface charge density on macroions adsorption are analyzed. Thus, we consider macroions ($\rho_M = 0.01$ M and $z_M = -10$) in (a) monovalent ($\rho_+ = 1.1$ M and $\rho_- = 1.0$ M) and (b) divalent ($\rho_+ = 0.55$ M and $\rho_- = 0.5$ M) electrolyte solutions. For each case, we considered two macroion sizes ($a_M = 3.8a$ and $a_M = 7a$) and three values for the membrane charge densities: (i) $\sigma_1 = \sigma_2 = 0.272$, (ii) $\sigma_1 = \sigma_2 = -0.272$, and (iii) $\sigma_1 = 0.68$, $\sigma_2 = -0.136$. Finally, we show calculations for the osmotic pressure (as a function of the macroion concentration) compared with experimental results.

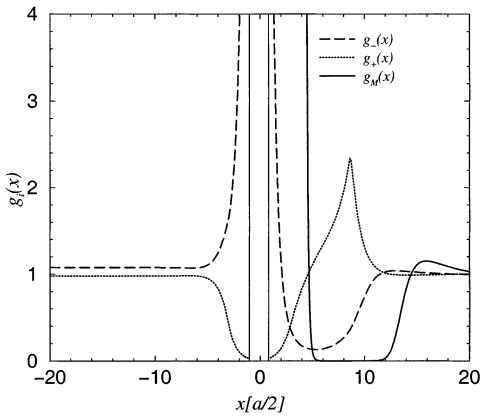

Figure 2. Reduced concentration profiles (RCPs) for a macroions solution ($\rho_M = 0.01$ M, $z_M = -10$) in a monovalent electrolyte ($\rho_+ = 1.1$ M and $\rho_- = 1.0$ M), with $a_3 = 3.8a$, $\sigma_1 = \sigma_2 = 0.272$, and $d = a$. The continuous, dashed, and dotted lines represent the RCPs for the macroions, anions, and cations, respectively.

3.1. Macroions in a Monovalent Electrolyte. In this subsection, we discuss the case of macroions ($z_M = -10$) in a monovalent electrolyte solution ($\rho_+ = 1.1$ M, $\rho_- = 1.0$ M, $z_+ = -z_- = 1$).

3.1.1. Positively Charged Membrane. In Figure 2, we present the RCPs when the membrane is positive and symmetrically charged ($\sigma_1 = \sigma_2 = 0.272$), where the membrane thickness is $d = a$ and $a_M = 3.8a$. As a result, we obtained the asymptotic values of the distribution functions in the α phase, $g_-(-\infty) = 1.0758$ and $g_+(-\infty) = 0.9779$, and demonstrated that the bulk electroneutrality condition (given by eq 9) is satisfied. In both phases, we observe that the negative ions are adsorbed and the positive ions expelled, as it is expected. In the β phase, at the membrane surface, the concentrations of macroions and small negative ions are $\rho_M((a_M + d)/2) \approx 20$ M and $\rho_-((a + d)/2) \approx 8.5$ M, respectively. Hence, the adsorption of macroions is more favorable than the adsorption of negative small ions. This is understood in terms of the electrostatic energy of one particle of species i at the membrane surface, U_i: because $|z_M| > |z_-|$, from eq 40, it is easy to see that $U_M < U_- < 0$, which favors macroions adsorption. As we pointed out above, many body correlations also influence adsorption. In this case, macroion−macroion long range correlations are predominantly more important than the ion−ion correlations because $\xi_{MM} \approx 7\xi_{--}$. A higher value of the macroion−macroion coulomb copling, ξ_{MM}, gives the appearance of a larger macroions size. Hence, the macroions excluded volume is higher, which increases macroions adsorption. Short-range correlations are also important and play an important role in the macroions adsorption: an increment of macroions concentration (keeping constant a_M

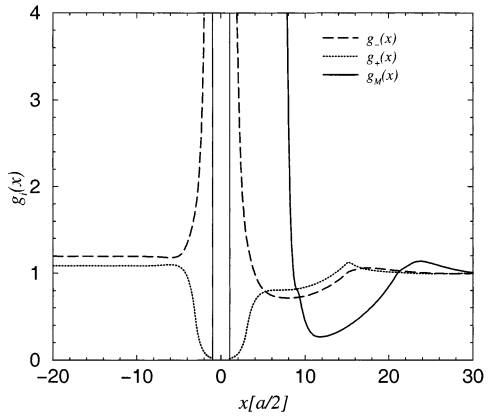

Figure 3. Same as in Figure 2 but with $a_3 = 7a$. The continuous, dashed, and dotted lines represent the RCPs for the macroions, anions, and cations, respectively.

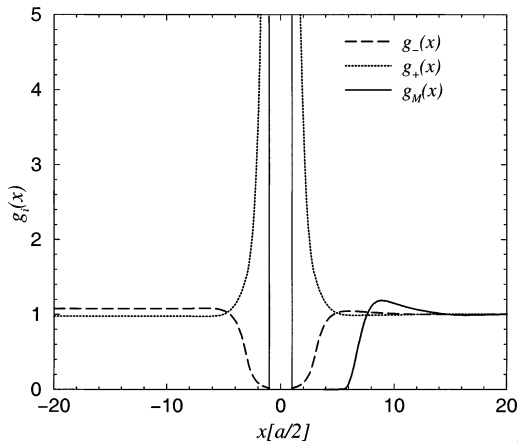

Figure 4. Reduced concentration profiles (RCPs) for a macroions solution ($\rho_M = 0.01$ M, $z_M = -10$) in a monovalent electrolyte ($\rho_+ = 1.1$ M and $\rho_- = 1.0$ M), with $a_3 = 3.8a$, $\sigma_1 = \sigma_2 = -0.272$, and $d = a$. The continuous, dashed, and dotted lines represent the RCPs for the macroions, anions, and cations, respectively.

and z_M) implies an increment of η_T and produces an increment of the macroions adsorption. However, an increment of η_T is not always followed by an increment of the adsorption as it will be noticed in the discussion of Figure 3. In Figure 2, we find a first macroions layer next to the membrane surface. After this layer there is a region where the macroions are completely expelled and then a small second peak (at $x \approx 15a/2 \approx 4a_M$) indicates the formation of a second macroions layer. The negative small ions are also adsorbed to the membrane's surface but their concentration is smaller than for the macroions, as pointed out above. The RCP for positive ions shows that these are completely expelled from the membrane right surface. However, a peak in the RCP is found at $x \approx 4.3a$ which is the ion−surface distance when there is a macroion inbetween. This peak implies an effective surface-cation attraction due to a *field inversion* caused by the surface CR.

Figure 3 shows the results obtained for the same system as in Figure 2 except that the macroions are larger, $a_M = 7a$. At the α phase, the distribution function have the same qualitative behavior as in Figure 2; however, in this case, $g_-(-\infty) = 1.1938$ and $g_+(-\infty) = 1.0853$; that is, the amount of salt in the α phase increases by increasing the macroions size. Because the particles excluded volume is increased, a higher amount of salt in the α phase is required to compensate the increment of the osmotic pressure at the β phase. The macroions concentration at the membrane surface is $\rho_M((d + a_M)/2) \approx 1.4$ M; thus, with respect to Figure 2, a decrement of macroions adsorption is observed in Figure 3. The increment of the macroions diameter implies a decrement of the macroions-macroions long-range correlations (in this case $\xi_{MM} \approx 2\xi_{--}$) and an increment of η_T, and hence, an increment of the contributions arising from correlations of short-range nature. Such an increment, however, is not sufficient to increase the macroions adsorption. This is understood in terms of eq 40 [$U_M(a_M = 3.8a) < U_M(a_M = 7a)$] which implies that the adsorption is energetically less favorable for $a_M = 7a$ than for smaller macroions with the same charge; that is, the driving mechanism for the macroions adsorption is the membrane−macroion electrostatic attraction. However, if the macroions surface charge density ($\sigma_M \equiv q_M/\pi a_M^2$) is kept constant, an increment of the macroions size implies an increment of their adsorption.

3.1.2. Negatively Charged Membrane. Figure 4 shows the RCPs when the membrane is negative and symmetrically charged ($\sigma_1 = \sigma_2 = -0.272$) for $a_M = 3.8a$. The membrane thickness is $d = a$. The asymptotic value of the distributions function *does not depend on the membrane's charge and thickness*; hence, the $g_i(-\infty)$ have the same value as in Figure 2. The RCPs for small ions behave in a normal way in the sense that positive ions are attracted to the membrane surface, whereas the negative ions are expelled from it. In the β phase, it is observed that macroions are expelled from the membrane surface for $x < 6(a/2)$. After this zero concentration region, an small peak in the macroions RCP is observed at $x \approx 9(a/2)$ indicating an effective macroion-membrane *attractive* force and an slight surface CR produced by the small cations. At these electrolyte conditions (1:1 and $\rho_+ = 1$M *with no macroions*), cations display a monotonically decaying distribution profile.[12] Hence, the oscillatory behavior of the RCPs for the small ions (in the β phase) is a consequence of the presence of macroions. By considering the macroions size $a_M = 7.0$ (not shown), the qualitative behavior of the RCPs is similar to that of Figure 4 with the following differences: (i) the RCPs oscillations of the small ions at the β phase are of *longer range* and (ii) the macroions RCP maximum is higher. These facts point out the relevance of the effect of the particles size and concentration (particles volume fraction) in the effective attraction between like charged particles in solution.[30−34]

From the analysis presented in Figures 2−4 we see that macroions adsorption increases by increasing η_T, ξ_{MM}, and $-U_M$. However, we point out the following findings: when macroions and the surface are oppositely charged, long-range electrostatic correlations dominate over short-range correlations. Hence, adsorption is enhanced by increasing ξ_{MM} and/or $-U_M$. On the other hand, when macroions and the surface are like charged, the mechanism for macroions adsorption (mediated by the small ions) is mainly driven by short-range correlations; thus, adsorption increases by increasing η_T even though ξ_{MM} decreases.

3.1.3. Unsymmetrically Charged Membrane. In Figure 5, the RCPs at the two membrane sides are shown for a macroions diameter $a_3 = 3.8a$ and $d = a$. The membrane is *unsymmetrically* charged with $\sigma_1 = 0.68$ and $\sigma_2 = -0.136$. At the right-hand side, surface macroions and small anions (negatively charged) are adsorbed on the membrane, despite $\sigma_2 < 0$. The adsorption of negatively charged particles on a negatively charged surface is due to the correlation between the two fluids. This is understood by considering the following two facts: (i) the membrane has a positive *net* charge ($\sigma_T > 0$) and (ii) the charge on the left-hand side surface (σ_1) is not completely screened by the excess of charge in its corresponding fluid phase (σ^α); that is, there is a violation of the local electroneutrality condition.[27−29,53] However, the overall electroneutrality condition

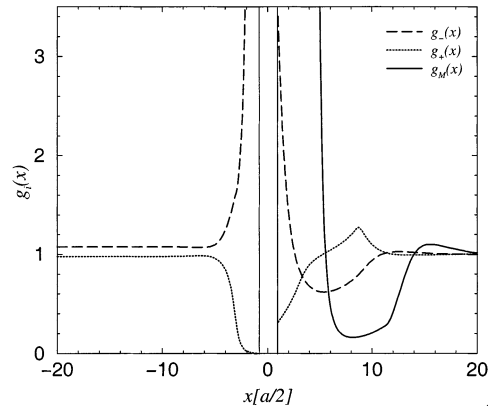

Figure 5. Reduced concentration profiles (RCPs) for a macroions solution ($\rho_M = 0.01$ M, $z_M = -10$) in a monovalent electrolyte ($\rho_+ = 1.1$ M and $\rho_- = 1.0$ M), with $a_3 = 3.8a$, $\sigma_1 = 0.68$, $\sigma_2 = -0.136$, and $d = a$. The continuous, dashed, and dotted lines represent the RCPs for the macroions, anions, and cations, respectively.

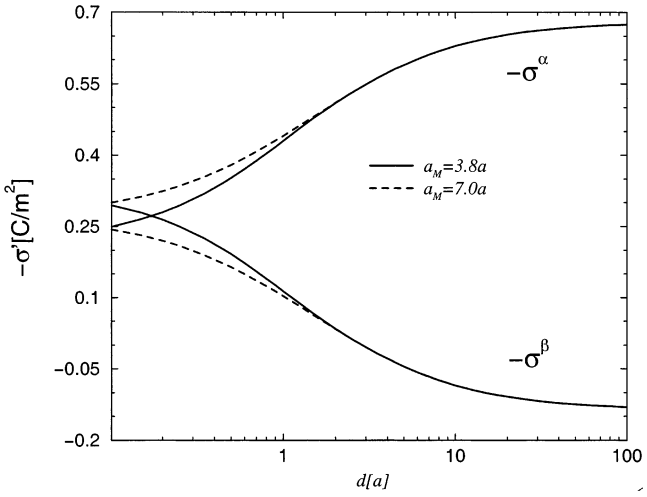

Figure 6. Induced charge densities as a function of the membrane thickness for a macroions solution ($\rho_M = 0.01$ M, $z_M = -10$) in a monovalent electrolyte ($\rho_+ = 1.1$ M and $\rho_- = 1.0$ M) with $\sigma_1 = 0.68$ and $\sigma_2 = -0.136$. The continuous line represents calculations for $a_M = 3.8a$, whereas the dashed line for $a_M = 7.0a$.

(eq 10) is satisfied. Therefore, the electric field produced by $\sigma_1 + \sigma^\alpha$ overcomes the field produced by σ_2, inducing macroions and anions adsorption. From here, we observed that σ^α and σ^β depend on d as it is discussed below.

In Figure 6, the induced charge densities σ_α and σ_β are shown, as a function of the membrane's thickness d. The dependence on the wall thickness of the induced charge densities σ_α and σ_β is a manifestation of the correlation between the fluids. The correlation between the two fluids is due to the electrostatic interaction among the particles at both phases but, more importantly, to the fact that they are at constant chemical potential. This phase−phase correlation also has been observed in fluids made of particles interacting via a short-range potential.[54] For a sufficiently large membrane's thickness, the induced charge density in each fluid phase screens its corresponding membrane surface, i.e., $\sigma^\alpha \to -\sigma_1$ and $\sigma^\beta \to -\sigma_2$ as $d \to \infty$. At $d = 100a$ each fluid has screened its respective surface charge density. Here we show a comparison between the results obtained for $a_M = 3.8a$ and $a_M = 7a$. In both cases, the results are qualitatively similar. However, the violation of the local electroneutrality condition is larger for the $a_M = 3.8a$ case, which is due to the stronger membrane−macroions interaction potential (U_M). Typically, $\epsilon \approx 6$ for a biological membrane. This would imply a stronger correlation of the fluids at both sides of the membrane. The consideration of the membrane dielectric constant (different to that of the fluid) may have important consequences for the membrane phenomenology. These effects will be addressed in a future research.

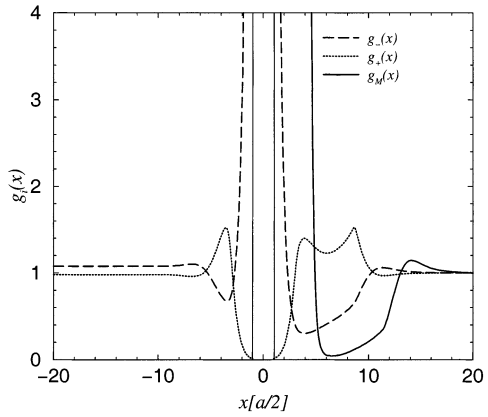

Figure 7. Reduced concentration profiles (RCPs) for a macroions solution ($\rho_M = 0.01$ M, $z_M = -10$) in a divalent electrolyte ($\rho_+ = 0.55$ M and $\rho_- = 0.5$ M), with $a_3 = 3.8a$, $\sigma_1 = \sigma_2 = 0.272$, and $d = a$. The continuous, dashed, and dotted lines represent the RCPs for the macroions, anions, and cations, respectively.

3.2. Macroions in a Divalent Electrolyte. We now discuss the case of macroions ($z_M = -10$) in a divalent electrolyte solution ($\rho_+ = 0.55$ M, $\rho_- = 0.5$ M, $z_+ = -z_- = 2$).

3.2.1. Positively Charged Membrane. In Figure 7, we show the RCPs for $\sigma_1 = \sigma_2 = 0.272$, $d = a$, and $a_M = 3.8a$. At the α phase, we observe oscillations of the RCPs, which is a typical behavior of a divalent electrolyte. Although we observe a strong adsorption of macroions in the β phase, the amount of adsorbed small negative ions is even larger (the concentrations of macroions and small negative ions at the interface are $\rho_M((d + a_M)/2) \approx 7.2$ M and $\rho_-((d + a)/2) \approx 16$ M, respectively). According to eq 40, macroion adsorption should be energetically more favorable; however, macroion adsorption is inhibited because divalent positive ions more efficiently screen macroion−membrane and macroion−macroion interactions. We infer this from the RCP for cations, which displays two small peaks at $x \approx 2a$ and $x \approx 4.3a$. The first peak corresponds to a positive ions layer contiguous to the negative ions adsorbed on the wall. The position of the second peak corresponds to a positive ions layer next to the macroions layer. This structure indicates that positive ions surround macroions due to their strong electrostatic interaction. In this case, $\xi_{M+} \approx -8.3(e^2/\epsilon k_B T a) \approx -14$, whereas for macroions in a monovalent electrolyte, $\xi_{M+} \approx -7$. By comparison of Figures 2 and 7 we see that macroions (next to an oppositely charged surface) are better adsorbed when they are in a monovalent solution rather than in a multivalent solution: for this particular case of macroions ($\rho_M = 0.01$ M, $z_M = -10$, and $a_M = 3.8a$), $\rho_M((d + a_M)/2) = 20$ M when macroions are in a monovalent electrolyte, whereas $\rho_M((d + a_M)/2) \approx 7.2$ M when macroions are in a divalent electrolyte. According to Figure 7, this is due to the reduction of the effective charge of the quasi-particles formed by the macroions and the small positive ions.

In Figure 8, we show the RCPs for the same conditions as in Figure 7 but $a_M = 7a$. Although macroions adsorb in the β phase, they do not influence significantly the local concentration of small ions. Hence, we see that the RCPs for small ions are quantitatively similar in both phases: the concentrations of counterions at the membrane surfaces are $\rho(\pm(d + a)/2) \approx 22.5$

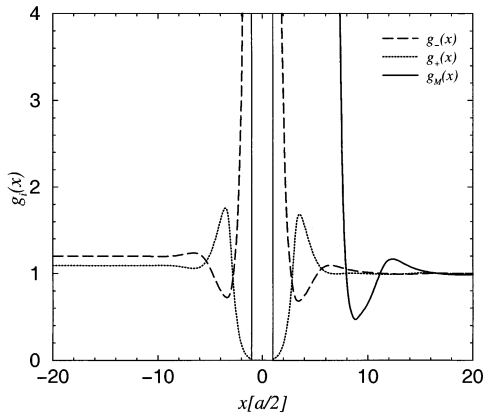

Figure 8. Same as in Figure 7 but with $a_3 = 7a$. The continuous, dashed, and dotted lines represent the RCPs for the macroions, anions, and cations, respectively.

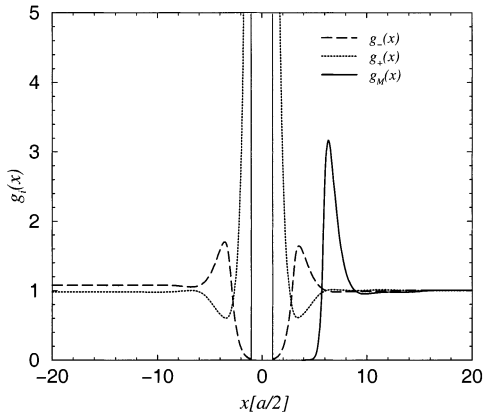

Figure 9. Reduced concentration profiles (RCPs) for a macroions solution ($\rho_M = 0.01$ M, $z_M = -10$) in a divalent electrolyte ($\rho_+ = 0.55$ M and $\rho_- = 0.5$ M), with $a_3 = 3.8a$, $\sigma_1 = \sigma_2 = -0.272$, and $d = a$. The continuous, dashed, and dotted lines represent the RCPs for the macroions, anions, and cations, respectively.

M, and in addition, the RCPs maxima are located symmetrically around $x \approx \pm 1.7a$. The adsorption of macroions decrease (with respect to Figure 7) due to the efficient screening of the membrane charge by the small negative ions and because the adsorption of larger ions (keeping z_M constant) is energetically less favorable, as it was pointed out in the discussion of Figure 3. We see that the layer of cations around macroions (seen in Figure 7) disappears possibly due to the decrement of their Coulombic interaction, in this case $\xi_{M+} \approx -8.4$.

3.2.2. Negatively Charged Membrane. In Figure 9, we show the RCPs for a negatively charged membrane ($\sigma_1 = \sigma_2 = -0.272$) with $d = a$ and $a_M = 3.8a$. The quantitative behavior of the small ions RCPs is similar at both phases, as much as the location of the maxima located symmetrically at $x \approx \pm 1.8a$. At the β phase, the macroions RCP displays a peak at $x = 3.2a$ indicating the formation of a macroions layer. The *adsorption* of macroions at this layer is enhanced (with respect to Figure 4) because of the surface *charge reversal* produced by the divalent cations; that is, macroions see the membrane surface with an effective positive charge. By increasing macroions size (keeping z_M constant), macroions attraction to an effective oppositely charged surface is energetically less favorable. Thus, we observe that macroions adsorption decreases by increasing macroions size, in opposition to the behavior of macroions (in a monovalent electrolyte solution) contiguous to a like charged surface, where the adsorption increases by increasing the macroions size (see the discussion of Figure 4).

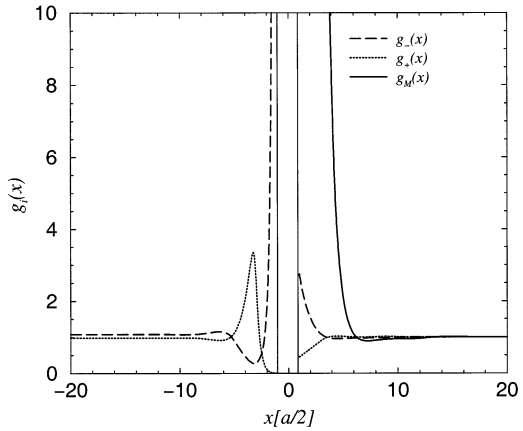

Figure 10. Reduced concentration profiles (RCPs) for a macroions solution ($\rho_M = 0.01$ M, $z_M = -10$) in a divalent electrolyte ($\rho_+ = 0.55$ M and $\rho_- = 0.5$ M), with $a_3 = 3.8a$, $\sigma_1 = 0.68$, $\sigma_2 = -0.136$, and $d = a$. The continuous, dashed, and dotted lines represent the RCPs for the macroions, anions, and cations, respectively.

This is due to the surface charge reversal produced by the divalent ions, which makes the macroions behave as if they were next to an oppositely charged surface (see discussion of Figures 2 and 3).

It seems to be a general feature that macroions next to an *oppositely* charged surface are better adsorbed when they are in a monovalent solution than in a multivalent solution. It is important to point out the formation of a cations layer around the macroions when $|\xi_{M+}|$ is high (seen for the divalent electrolyte in Figure 7). On the other hand, when macroions and the surface are like charged, a *divalent* electrolyte solution mediates an effective membrane-macroions attraction, this attraction is favored by a higher value of ξ_{MM} rather than for a high value of η_T, as in the monovalent case.

3.2.3. Unsymmetrically Charged Membrane. In Figure 10, we show the RCPs at the two phases for $\sigma_1 = 0.68$, $\sigma_2 = -0.136$, $a_3 = 3.8a$, and $d = a$. The correlation between the two fluids is manifested by the attraction of negatively charged particles toward the negatively charged surface at the α phase. However, the adsorption of macroions is quite less efficient than in the monovalent electrolyte case of Figure 5: In the monovalent case, the contact value of the local concentration is $\rho_M((d + a_M)/2) \approx 2.7$ M, whereas in this case, it is $\rho_M((d + a_M)/2) \approx 0.12$ M. This is due mainly to the more efficient field screening by the divalent electrolyte at the left-hand side surface. In the monovalent electrolyte case, the induced charge density at the α phase is $\sigma_\alpha = -0.43$ when $d = a$, whereas in the divalent electrolyte, case $\sigma_\alpha = -0.50$.

3.3. Osmotic Pressure. Although the adsorption of macroions is strongly influenced by the membrane surface charge and thickness, we observe, however, that the osmotic pressure does not depend on these membrane properties as it has been pointed out in subsection 2.3. In Figure 11, we show the osmotic pressure (obtained from HNC/MS theory) as a function of the macroion concentration, ρ_M, for two macroion sizes. This plot shows the osmotic pressure for macroions in a monovalent electrolyte and in a divalent electrolyte.

The osmotic pressure increases by increasing the particles excluded volume (either ρ_M or a_M). On the other hand, an important quantitative difference between the curves for the osmotic pressure of macroions in a monovalent and divalent electrolytes is observed. However, the increment of the osmotic pressure produced by increasing the macroions size is more significant and is due to the increment of the particles excluded

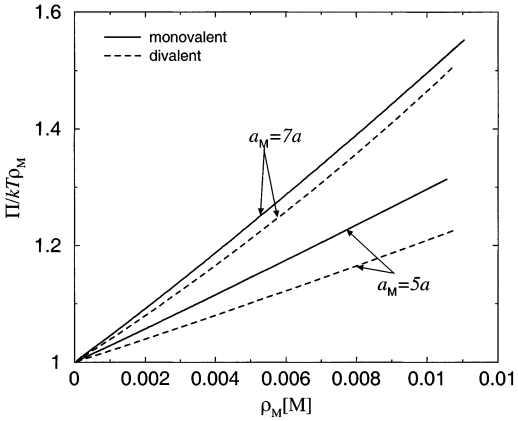

Figure 11. Reduced osmotic pressure as a function of the macroions concentration, ρ_M, for $z_M = -10$ and two macroion sizes, $a_M = 5a$ and $a_M = 7a$. The solid lines represents the osmotic pressure for macroions in a monovalent electrolyte ($\rho_- = 1.0$ M), whereas the dashed lines represent the osmotic pressure for macroions in a divalent electrolyte ($\rho_- = 0.5$ M).

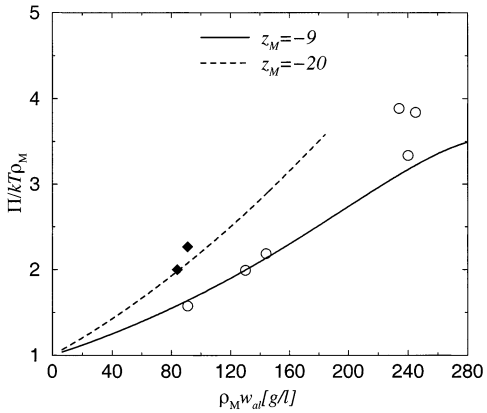

Figure 12. Bovine serum albumin reduced osmotic pressure as a function of albumin weight concentration, $\rho_M w_{al}$, at 25 °C and in 0.15 M NaCl at pH = 7.4 ($Q = -20e$) and pH = 5.4 ($-9e$) from ref 6. The curves are obtained from eq 12 using $a_M = 62$ Å, $a = 4.25$ Å, and $z = 1$.

volume. As we pointed out above (see the discussion of Figure 4), a higher particles charge conferees a higher excluded volume to particles; hence, the ionic charge plays a role similar to short-range correlations: an increase of the particles charge (either, macroions, or salt) will produce an increment of the osmotic pressure. This fact is, however, not manifested in Figure 11 (for the same value of a_M) because the salt concentration is lower in the divalent case than in the monovalent case.

Computation of the osmotic pressure of proteins solutions is an issue addressed by some authors.[7,55] Results of particular interest are those for albumin solutions, for which theoretical calculations and measurements of the osmotic pressure have been reported. In Figure 12, we show the osmotic pressure predictions of HNC/MS theory (as a function of the protein concentration) and experimental results.

The experimental data correspond to a solution of albumin in a 0.15 M NaCl aqueous solution. In accordance with titration measurements, the albumin has a net charge of $Q = -9e$ and $Q = -20e$ for pH $\approx$ 5.4 and pH $\approx$ 7.4, respectively. In our calculations, we have used $a_M = 62$ Å which corresponds to the experimental protein diameter. The good agreement between theory and experiment is remarkable as well as the fact that no adjustable parameters have been used.

The prediction of HNC/MS fits well the experimental data even for a protein concentration as high as 30% the protein volume in solution (which is estimated assuming the albumin molecular weight $w_{al} = 69$ Kg/mol). For very high protein concentrations ($\rho_M w_{al} > 280$ g/l), HNC/MS shows discrepancies with experimental measurements which may be associated with the following facts: (i) the albumin molecule is not *spherically* symmetric as in the model, therefore, the protein geometry becomes relevant when the protein volume fraction is high, (ii) integral equations are approximated theories, meaning that they do not take into account all the particle correlations.

4. Conclusions

We studied a simple model charged membrane separating two fluid phases (α and β). The β phase contains macroions in an electrolyte solution, and the α phase is a simple electrolyte solution. The system is modeled in such a way that the small ions at both phases are at the same chemical potential; thus, the membrane is considered to be semipermeable. We considered explicitly the effect of short and long-range correlations, through the hypernetted chain/mean spherical (HNC/MS) integral equation. By a simple force balance, we derived the expression for the osmotic pressure in terms of the ions reduced concentration profiles. With the solution of the HNC/MS integral equations, we obtained the particles concentration profiles, to study the adsorption of macroions on the membrane and the solution osmotic pressure.

We analyzed the influence of the membrane surface charge density, membrane thickness, the effect of salt valence, and the effect of macroions charge, size, and concentration. (1) When the membrane and macroions are oppositely charged, a larger value of σ_T or z_M implies a larger adsorption, because it is energetically more favorable. In the case of z_M, the larger adsorption is also due to an increase of the macroions counterion concentration in the β phase, because η_T increases; that is, there is, in addition, an entropy driven adsorption mechanism. However, for larger macroion diameters, i.e., larger η_T, in a monovalent electrolyte (keeping the same macroions charge and concentration), the adsorption is less favorable because the ion−membrane surface energy interaction, U_M, increases; that is, it is less negative. This is so because, for larger macroions, the macroion charge density decreases and, hence, the membrane-macroion electrostatic interaction decreases. If the macroions are in a 2:2 electrolyte, they are surrounded by their counterions and form complexes which screen the membrane−macroions attractive interaction. In addition, divalent counterions are in a lower concentration and, thus, η_T is lower. Thus, macroions adsorption is less favorabe when their counterions are multivalent than when they are monovalent.

(2) The attraction of macroions, in a monovalent electrolyte, toward a *like-charged* surface is energetically unfavorable. Nevertheless, in our model, we find that such an attraction is favored by an *intermediate* layer of small ions and, mainly, by the macroion−macroion short-range correlations. In this case, an increase of macroions size *does* imply a larger macroions adsorption. If the macroions are in a divalent electrolyte solution, the multivalent membrane counterions produce a surface charge reversal. Therefore, macroions behave as if they were contiguous to an oppositely charged surface which increases macroions adsorption, to the layer of counterions next to the membrane.

(3) As a consequence of the permeability condition and constant chemical potential, we have that for an unsymmetrically

charged membrane the fluids *correlation* may produce *direct adsorption* of charged macroions on a *like charged surface*. This is due to the fact that the surface charge density of one of the membrane's surface is not canceled by the induced charge in its correspondig fluid phase, i.e., there is a violation of a local electroneutrality condition. This fact implies a non trivial relation between the induced charge densities (σ^{α} and σ^{β}) and the membrane thickness. It should be pointed out that a violation of the local electroneutrality condition on the α phase implies a different adsorption of macroions to the membrane than that in an infinitely thick membrane.

In studying the osmotic pressure, we looked at the effect of particles excluded volume and (macroions and salt) charge. The salt concentration at the α phase (ρ_i^{α}) is a result from our theory, in contrast with the classical Donnan equilibrium theory. We found the expected result that an increment of the osmotic pressure produce an increment of ρ_i^{α}. In general, an increment of macroions size produces an increment of the osmotic pressure and an increment of the salt concentration at the α phase. In any case, as a general result of our study, a higher osmotic pressure implies a higher macroions adsorption either, direct or mediated by small counterions. The opposite is also true: a higher adsorption implies a higher osmotic pressure, with the exception of a higher adsorption due to an increment of the membrane surface charge, in which case no increment of osmotic pressure occurs. Charge conferees to the particles (either, salt ions or macroions) a higher effective excluded volume due to the electrostatic repulsion. Thus, an increment of the charge is followed by an increment of the salt concentration at the α phase and hence of the osmotic pressure. The theory predictions are robust as it is shown by the good agreement between theory and experiment, where we have not used adjustable parameters. The results of this work could be technologically relevant for the design of selective membranes.[56]

Acknowledgment. We gratefully acknowledge the financial support of INDUSTRIAS NEGROMEX.

Appendix A

A.1. Mean Spherical Closure. The primitive model is the simplest model for an electrolyte that includes some of the most relevant aspects of real solutions. In the general case, the primitive model is constituted by n species of particles, with the mixture is embedded in a uniform medium of dielectric constant ϵ at temperature T. Each species is defined by the particles point charge at the center, $q_i = z_i e$ (where e stands for the proton's charge and z_i for the ionic valence), the ionic diameter, a_i, and number concentration, ρ_i. The fluid is constrained to the following condition

$$\sum_{i=1}^{n} z_i \rho_i = 0 \tag{43}$$

The expressions for the direct correlation functions, $c_{ij}(r_{13})$, for a *bulk* electrolyte (required in n eq 6) were obtained by Blum[57] and Hiroike,[58] through the MS closure, and are written as

$$c_{ij}(r_{13}) = \frac{e^2\beta}{\epsilon} d_{ij}(r_{13}) + c_{ij}^{\mathrm{hs}}(r_{13}) - \beta \frac{z_i z_j e^2}{\epsilon r_{13}} \tag{44}$$

with $c_{ij}^{sr}(r_{13}) = (e^2\beta/\epsilon) d_{ij}(r_{13})$, $\beta = 1/k_B T$ and

$$d_{ij}(r_{13}) = b_{ij}^{(1)} + \frac{z_i z_j}{r_{13}}, \text{ for } 0 \le r_{13} \le \lambda_{ij}$$

$$\frac{b_{ij}^{(2)} + z_i z_j}{r_{13}} - b_{ij}^{(3)} + b_{ij}^{(4)} r_{13} + b_{ij}^{(5)} r_{13}^3, \text{ for } \lambda_{ij} < r_{13} \le a_{ij}$$

$$0, \text{ for } r_{13} > a_{ij} \tag{45}$$

with $\lambda_{ij} \equiv |a_i - a_j|/2$ and $a_{ij} \equiv (a_i + a_j)/2$. The constants in eq 45 are given by

$$s_i = (n_i + \Gamma x_i)$$

$$b_{ij}^{(1)} = 2\left[z_i n_j - x_i s_i + \frac{a_i}{3} s_i^2\right]$$

$$b_{ij}^{(2)} = (a_i - a_j)\left\{\frac{(x_i + x_j)}{4}[s_i - s_j]\right.$$

$$\left. - \frac{(a_i - a_j)}{16}[(n_i + \Gamma x_i + n_j + \Gamma x_j)^2 - 4 n_i n_j]\right\}$$

$$b_{ij}^{(3)} = (x_i - x_j)(n_i - n_j)$$

$$+ (x_i^2 + x_j^2)\Gamma + (a_i + a_j) n_i n_j - \frac{1}{3}[a_i s_i^2 + a_j s_j^2]$$

$$b_{ij}^{(4)} = \frac{x_i}{a_i} s_i + \frac{x_j}{a_j} s_j + n_i n_j - \frac{1}{2}[s_i^2 + s_j^2]$$

$$b_{ij}^{(5)} = \frac{s_j}{6 a_j^2} + \frac{s_i}{6 a_i^2}$$

where x_i are defined as $x_i \equiv z_i + n_i a_i$ and Γ is obtained from the solution of the following algebraic equation

$$\Gamma^2 = \frac{\pi e^2 \beta}{\epsilon} \sum_{i=1}^{n} \rho_i (z_i + n_i a_i)^2 \tag{46}$$

The n_i are obtained from the solution of the following set of algebraic equations

$$-(z_i + n_i a_i)\Gamma = n_i + c a_i \sum_{j=1}^{n} (z_i + n_j a_i) \tag{47}$$

where $c = (\pi/2)[1 - (\pi/6)\sum_{j=1}^{n} \rho_i a_i^3]^{-1}$.

Considering that $a = a_1 = a_2$, $c_{ij}^{\mathrm{hs}}(r_{13})$ is just the direct correlation function for a hard spheres *binary* mixture in the PY approximation. For particles of the same size, it is given by[59]

$$c_{ii}^{\mathrm{hs}}(r_{13}) = \begin{bmatrix} -A_i - B_i r_{13} - \delta r_{13}^3 & \text{for } r_{13} < a_i \\ 0 & \text{for } r_{13} > a_i \end{bmatrix} \tag{48}$$

For particles of different sizes, we have

$$c_{13}^{\mathrm{hs}}(r_{13}) = \begin{bmatrix} -A_1 & \text{for } s \le \lambda_{13} \\ -A_1 - \dfrac{[\alpha x^2 + 4\lambda_{13}\delta x^3 + \delta x^4]}{r_{13}} & \text{for } \lambda_{13} < r_{13} \le a_{13} \\ 0 & \text{for } r_{13} > a_{13} \end{bmatrix} \tag{49}$$

with $x \equiv r_{13} - \lambda_{13}$. The constants used in eqs 48 and 49 are given by

$$A_1 = (1-\eta_T)^{-3}\left\{1 + \eta_T + {\eta_T}^2 + \frac{\pi}{6}a^3\rho_T[1+2\eta_T] - \frac{\pi}{2}\rho_3(a_3-a)^2\{a(1+\eta_3)+a_3[1+2(\eta_1+\eta_2)]\}\right\} + \frac{\pi a^3}{2}(1-\eta_T)^{-4}\left\{\rho_T(1+\eta_T+{\eta_T}^2) - \frac{\pi}{2}\rho_3(\rho_1+\rho_2)(a_3-a)^2\left[(a+a_3)+aa_3\frac{\pi}{6}\sum_{i=1}^{3}\rho_i{a_i}^2\right]\right\} \quad (50)$$

$$\alpha = -\pi a_{13} g_{13}(a_{13})\sum_{i=1}^{3}\rho_i a_i g_{ii}(a_i) \quad (51)$$

$$\delta = \frac{\pi}{12}\sum_{i=1}^{3}\rho_i A_i \quad (52)$$

$$B_1 = B_2 = -\pi[(\rho_1+\rho_2)a^2 g_{11}^2(a) + \rho_3 a_3 g_{13}^2(a_{13})] \quad (53)$$

with

$$g_{11}(a) = g_{22}(a) = \left\{\left[1+\frac{1}{2}\eta_T\right] + \frac{3}{2}\eta_3 a_3^3(a-a_3)\right\}(1-\eta_T)^{-2}$$

$$g_{13}(a_{13}) = \frac{[a_3 g_{11}(a) + a g_{33}(a_3)]}{2a_{13}} \quad (54)$$

The expressions for A_3, B_3, and $g_{33}(a_3)$ are obtained by interchanging $\eta_1 + \eta_2$, $\rho_1 + \rho_2$, and a_1 with η_3, ρ_3, and a_3, respectively, in the expressions for A_1, B_1, and $g_{11}(a)$.

A.2. Kernels Expressions. Carrying out the integrations indicated in eqs 20 and 21, using eqs 45, 48, and 49, the expressions for $K_{ij}(x, y)$ and $D_{ij}(x, y)$ are

$$D_{ij}(x,y) = b_{ij}^{(1)} k_0 + z_i z_j J_1 + b_{ij}^{(2)} M_1 - b_{ij}^{(3)} M_2 + b_{ij}^{(4)} M_3 + b_{ij}^{(5)} M_5, \text{ for } 0 \le |x-y| \le \lambda_{ij}$$

$$(b_{ij}^{(2)} + z_i z_j)J_1 - b_{ij}^{(3)} J_2 + b_{ij}^{(4)} J_3 + b_{ij}^{(5)} J_5, \text{ for } \lambda_{ij} < |x-y| \le a_{ij}$$

$$0, \text{ for } a_{ij} < |x-y| \quad (55)$$

$$-K_{ii}(x,y) = A_i J_2 + B_i J_3 + \delta J_5, \text{ for } a_{ii} \ge |x-y|$$

$$0, \text{ for } a_{ii} < |x-y| \quad (56)$$

$$-K_{13}(x,y) = A_1 J_2 + \alpha a^3/3 + \delta\lambda_{13}a^4 + \delta a^5/5, \text{ for } |x-y| < \lambda_{13}$$

$$A_1 J_2 + \alpha P_3 + 4\delta\lambda_{13}P_4 + \delta P_5, \text{ for } \lambda_{13} < |x-y| \le a_{13}$$

$$0, \text{ for } a_{13} < |x-y| \quad (57)$$

where we use the following definitions:

$$J_n = ({a_{ij}}^n - |x-y|^n)/n \quad (58)$$

$$P_n = (a^n - (|x-y| - \lambda_{ij})^n)/n \quad (59)$$

$$M_n = ({a_{ij}}^n - {\lambda_{ij}}^n)/n \quad (60)$$

and

$$k_0 = ({\lambda_{ij}}^2 - (x-y)^2)/2 \quad (61)$$

References and Notes

(1) Hoppe, W. *Biophysics*; Springer Verlag: Berlin, 1983.
(2) Hiemenz, P. C. *Principles of Colloids and Surface Chemistry*; Marcel Dekker: New York, 1977.
(3) Tanford, C. *Physical Chemistry of Macromolecules*; John Wiley and Sons: New York, 1961.
(4) Donnan, F. G. *Z. Elektrochemistry* **1911**, *17*, 572.
(5) Guggenheim, E. A. *Theromodynamics: An Advanced Treatment for Chemists and Physicists*; North-Holland Physics Publishing: Amsterdam, 1967.
(6) Vilker, V. L.; Colton, C. K.; Smith, K. A. *J. Colloid Interface Sci.* **1981**, *79*, 548.
(7) Yousef, M. A.; Datta, R.; Rodgers, V. G. J. *J. Colloid Interface Sci.* **1998**, *207*, 273.
(8) Gouy, G. *J. Phys.* **1910**, *9*, 457.
(9) Chapman, D. L. *Philos. Mag.* **1913**, *25*, 475.
(10) Cuvillier, N.; Rondelez, F.; *Thin Solid Films* **1998**, *327−329*, 19.
(11) Torrie, G. M.; Valleau, J. P. *J. Chem. Phys.* **1980**, *73*, 5807.
(12) Lozada-Cassou, M.; Saavedra-Barrera, R.; Henderson, D. *J. Chem. Phys.* **1982**, *77*, 5150.
(13) Svensson, B.; Joensson, B.; Woodward, C. E. *J. Phys. Chem.* **1990**, *94*, 2105.
(14) Percus, J. K. In *The Equilibrium Theory of Classical Fluids*; Frisch, H. L., Lebowitz, J. L., Eds.; W. A. Benjamin: New York, 1964; Chapter II, p 33.
(15) Evans, R. In *Fundamentals of Inhomogeneous Fluids*; Henderson, D., Ed.; Marcel Dekker Inc.: New York, 1992; Chapter 3.
(16) Zhang, M. Q.; Percus, J. K. *J. Chem. Phys.* **1990**, *92*, 6799.
(17) Henderson, D.; Abraham, F. F.; Barker, J. A. *Mol. Phys.* **1976**, *31*, 1291.
(18) Lozada-Cassou, M. *J. Chem. Phys.* **1981**, *75*, 1412.
(19) Plischke, M.; Henderson, D. *Electrochim. Acta* **1981**, *34*, 1863.
(20) Greberg, H.; Kjellander, R. *Mol. Phys.* **1994**, *83*, 789.
(21) Attard, P. *Adv. Chem. Phys.* **1996**, *92*, 1.
(22) Decher, G. *Science* **1997**, *277*, 1232.
(23) Tohver, V.; Smay, J. E.; Braun, P. V.; Lewis, J. A. *PNAS* **2001**, *98*, 8950.
(24) Zhou Y.; Stell, G. *J. Chem. Phys.* **1988**, *89*, 7010.
(25) Zhou Y.; Stell, G. *J. Chem. Phys.* **1988**, *89*, 7020.
(26) The cavity is immersed in a two component electrolyte plus one macroion species, where the macroions are restricted to be outside the cavity whereas the electrolyte can permeate it.
(27) Lozada-Cassou M.; Yu, J. *Phys. Rev. Lett.* **1996**, *77*, 4019.
(28) Lozada-Cassou M.; Yu, J. *Phys. Rev. E* **1997**, *56*, 2958.
(29) Aguilar, G. E.; Lozada-Cassou, M.; Yu, J. *J. Colloid Interface Sci.* **2002**, *254*, 141.
(30) Muthukumar, M. *J. Chem. Phys.* **1996**, *105*, 5183.
(31) Crocker, J. C.; Matteo, J. A.; Dinsmore, A. D.; Yodh, A. G. *Phys. Rev. Lett.* **1999**, *82*, 4352.
(32) Kepler, G. M.; Fraden, S. *Phys. Rev. Lett.* **1994**, *73*, 356.
(33) Crocker, J. C.; Grier, D. G. *Phys. Rev. Lett.* **1996**, *77*, 1897.
(34) Han Y.; Grier, D. G. *Phys. Rev. Lett.* **2003**, *91*, 038302.
(35) Bolhuis, P. G.; Louis, A. A.; Hansen, J. P. *Phys. Rev. Lett.* **2002**, *89*, 128302.
(36) Trokhymchuk, A.; Henderson, D.; Nikolov, A.; Wasan, D. T. *Phys. Rev. E* **2001**, *64*, 012401.
(37) Jiménez-Ángeles F.; Lozada-Cassou, M. see cond-mat/0309446 at http://www.arxiv.org.
(38) Lozada-Cassou, M. In *Fundamentals of Inhomogeneous Fluids*; Henderson, D., Ed.; Marcel Dekker: New York, 1993; Chapter 8.
(39) Hansen J. P.; McDonald, I. R. *Theory of Simple Liquids*, 2nd ed.; Academic Press: London, 1986.
(40) Degrève, L.; Lozada-Cassou, M.; Sánchez, E.; González-Tovar, E. *J. Chem. Phys.* **1993**, *98*, 8905.
(41) Lozada-Cassou, M.; Olivares, W.; Sulbarán, B.; *Phys. Rev. E* **1996**, *53*, 522.
(42) Degrève, L.; Lozada-Cassou, M. *Phys. Rev. E* **1998**, *57*, 2978.
(43) Deserno, M.; Jiménez-Ángeles, F.; Holm, C.; Lozada-Cassou, M. *J. Chem. Phys.* **2001**, *105*, 10983.
(44) Lozada-Cassou, M. *J. Chem. Phys.* **1984**, *80*, 3344.
(45) Lozada-Cassou, M.; Dıaz-Herrera, E. *J. Chem. Phys.* **1990**, *92*, 1194.
(46) Olivares, W.; McQuarrie, D. A. *J. Phys. Chem.* **1980**, *84*, 863.
(47) Carnie, S. L.; Chan, D. Y. C. *J. Chem. Phys.* **1981**, *74*, 1293.
(48) Attard, P. *J. Phys. Chem.* **1995**, *99*, 14174.
(49) Greberg H.; Kjellander, R. *J. Chem. Phys.* **1998**, *108*, 2940.

(50) Jiménez-Ángeles, F.; Lozada-Cassou, M. see cond-mat/0303519 at http://www.arxiv.org.
(51) Lozada-Cassou, M.; Dıaz-Herrera, E. *J. Chem. Phys.* **1990**, *93*, 1386.
(52) Mier-y-Teeran, L.; Díaz-Herrera, E.; Lozada-Cassou, M.; Saavedra-Barrera, R. *J. Comput. Phys.* **1989**, *84*, 326.
(53) Lozada-Cassou, M.; Olivares, W.; Sulbarán, B.; Yu, J. *Physica A* **1996**, *231*, 197.
(54) Olivares, W.; Degrève, L.; Villegas, J. C.; Lozada-Cassou, M. *Phys. Rev. E* **2002**, *65*, 061702.
(55) Deserno, M.; von Grünberg, H.-H. *Phys. Rev. E* **2002**, *66*, 011401.
(56) *Membranes Technology*; Nunes, S. P., Peinemann, K.-V., Eds.; Wiley-VCH: Weinheim, Germany, 2001.
(57) Blum, L. *Mol. Phys.* **1975**, *30*, 1529.
(58) Kazuo, H. *Mol. Phys.* **1977**, *33*, 1195.
(59) Lebowitz, J. L. *Phys. Rev.* **1964**, *133*, A895.